Los Alamos National Laboratory is operated by the University of California for the United States Department of Energy under contract W-7405-ENG-36.

LA-UR--92-313

DE92 007409

TITLE: DUCTILE PHASE TOUGHENING OF MOLYBDENUM BY LOW PRESSURE PLASMA SPRAYING

AUTHOR(S): Richard Castro, MST-6
Ronald W. Smith, Drexel University
Anthony D. Rollett, MST-6
Paul W. Stanek, MST-6

SUBMITTED TO: Workshop on High Temperature Structural Silicides, Gaithersburg, MD, November 4-6, 1992; Materials Science & Engineering (to be published)

Los Alamos

Los Alamos National Laboratory
Los Alamos, New Mexico 87545

ABSTRACT

The low fracture toughness of $MoSi_2$ at ambient temperature has prompted investigations into new processing methods in order to impart some degree of fracture toughness into this inherently brittle material. In the following investigation, low pressure plasma spraying was employed as a fabricating technique to produce spray-formed deposits of $MoSi_2$ and ductile reinforced $MoSi_2$ composites containing approximately 10 and 20 volume percent of a discontinuous tantalum lamelli reinforcement. Fracture toughness (K_{1c}) measurements of $MoSi_2$ and the $MoSi_2$/Ta composites were done using a chevron notched 4-point bend fracture toughness test in both the as-sprayed condition and after hot isostatic pressing at 1200 °C/206 MPa for 1 hour. Results from the ductile reinforced $MoSi_2$/Ta composites have shown fracture toughness increases on the order of 200% over the as-sprayed $MoSi_2$ (4.50 $\pm$ 0.173 MPa $m^{1/2}$ to 9.97 $\pm$ 0.25 MPa $m^{1/2}$). In addition, a marked anisotropy in fracture toughness was observed in the spray-formed deposits due to the layered splat structure produced by the low pressure plasma spray process.

Ductile Phase Toughening of Molybdenum Disilicide by Low Pressure Plasma Spraying

Richard G. Castro[1], Ronald W. Smith[2], Anthony D. Rollett[1] and Paul W. Stanek[1]

[1]Material Science and Technology Division
Los Alamos National Laboratory, Los Alamos, NM 87544, USA
[2]Materials Engineering Department, Drexel University, Philadelphia, PA 19104, USA

1. INTRODUCTION

Intermetallic matrix composites have attracted attention for many high temperature structural applications because of properties such as higher melting points, lower densities and excellent oxidation and corrosion resistance. Over the past decade, research and development efforts have narrowed down the number of potential intermetallic compounds for high temperature applications [1]. Candidate materials such as aluminides and silicides have been identified as potential materials due to their oxidation resistance at high temperatures. One of the most promising intermetallic compounds, in the class of silicides, is molybdenum disilicide ($MoSi_2$). This compound has been known as a high melting intermetallic (2030 °C) for more than eighty years [2]. It has been used extensively in industry for non-structural applications such as protective coatings and electric heating elements because of its superior oxidation resistance in air and its ability to carry current.

One of the properties which has limited the application of $MoSi_2$ is its inherent lack of ductility at ambient temperatures. This brittle behavior has limited its use for many structural applications and has also hindered the study of its properties because of processing difficulties in fabricating specimens. Current materials research initiatives are focusing on new techniques which would help to overcome the brittle nature of $MoSi_2$. One technique which has shown significant promise in improving the ductility and toughness of brittle materials has been the use of ductile phase toughening as a mechanism to increase the fracture toughness of the material. By utilizing the high energy to failure of a uniform distributed ductile reinforcement in a brittle matrix, substantial improvements in fracture toughness have been achieved [3,4].

Plasma spraying as a means of fabricating composite and monolithic structures of metallic, intermetallic, and silicide systems has recently been demonstrated by a number of researchers [5,6,7]. Many of the unique structures and properties that have been obtained through this processing method are a consequence of the microstructure that results from the spray deposition process. The smaller matrix grains, chemical homogeneity and uniform distribution of second phases, have produced increases in yield strength, ultimate strength, thermal fatigue strength and fracture toughness, when compared to those of conventionally processed material. In addition, plasma spraying has been shown to be capable of producing near-net shapes of various geometries [5,8]. In this investigation, low pressure plasma spray forming was used as a fabricating technique to produce spray-formed deposits of $MoSi_2$ and discontinuous ductile reinforced $MoSi_2$/tantalum composites. The combination of the microstructure produced during plasma spraying and the additions of the discontinuous tantalum reinforcement, has resulted in substantial increases in the room temperature fracture toughness. Results from this investigation will be compared to fracture toughness values obtain by conventional hot pressing operations.

2.0 Experimental

2.1 Low Pressure Plasma Spraying

In fabricating spray-formed deposits of $MoSi_2$ and $MoSi_2$/Ta composites, the low pressure plasma spray facility at Los Alamos National Laboratory was used. This plasma spray facility contains a SG-100 Plasmadyne spray torch which is mounted inside a modified electron beam welding chamber. The welding gun and substrate fixturing were modified to accommodate the D.C. plasma spray torch and water cooled substrate holder. In spray forming the $MoSi_2$ and the $MoSi_2$/Ta deposits, two powder feed hoppers were used. One powder hopper contained a $MoSi_2$ powder feed stock (Metco powder

SP10542, 99.5% pure, Metco Inc. Westbury, L.I., N.Y.), while the other was subsequently loaded with either one of two different blends of $MoSi_2$ and tantalum powders (Kennametal tantalum powder B-185, 99.5 % pure, Latrobe, PA.,):

$MoSi_2$-10 w/o Ta

$MoSi_2$-20 w/o Ta

A particle size distribution of -200 +325 mesh (75 to 45 micrometers) with an average particle size of 60 micrometers was used for the $MoSi_2$ and Ta feed stock powders. These powders were internally injected into the spray torch during the plasma spraying operation. Optimization of the plasma spray parameters for this investigation was done by controlling the net energy of the plasma, the primary, secondary, and powder gas flow rates, and the powder mass flow into the plasma torch. The spray conditions were optimized based on as-deposited densities which were measured after systematically varying the primary gas flow (argon), secondary gas flow (helium), powder carrier gas flow (argon) and the system input power. Experimental details associated with this optimization study which yielded consistent as-deposited densities greater than 97% of $MoSi_2$ theoretical density (6.05 g/cc) can be found in reference [9]. The optimized spray conditions used to produce thick spray deposits of $MoSi_2$ and $MoSi_2$/Ta are given in Table 1.

Free standing forms of approximately (6.0 mm) thick by (90 mm) long were produced for both $MoSi_2$ and $MoSi_2$/Ta using the optimized conditions in Table 1. Spray deposits were produced on a (3.20 mm) thick Ta alloy substrate and were subsequently removed by lightly tapping the back of the substrate after the spray deposits reached room temperature. Figure 1 shows a representative sample produced by the low pressure plasma spray process. This figure shows a bell-shaped distribution of the deposit that results when continuously traversing the substrate back and forth along one direction under the plasma spray torch. Samples for microstructural characterization and fracture toughness were taken from the thickest regions of the bell-shaped spray-formed deposits. Thin foils for transmission electron microscopy (TEM) of the spray deposits were prepared by conventional slicing, polishing, dimpling, and ion milling in a Gatan Duo-Mill. TEM was performed on a Philips CM30 operating at 300 kV.

2.2 Fracture Toughness Testing

The room temperature fracture toughness (K_{IC}) of $MoSi_2$ and the $MoSi_2$/Ta composites were determined by using a chevron v-notched 4-point bend fracture toughness test. A review of this sample geometry and test method for K_{IC} measurements is given in reference [10]. The equation that relates the fracture toughness (K_{IC}) to the maximum load (P_{max}) obtained during the 4-point bend test is the following:

$$K_{1c} = A \cdot P_{max} \qquad (1)$$

where (A) is a test constant dependent on the specimen geometry and the manner of loading. An approximation for (A) is given by Munz et al., [11,12] which relates K_{1c} and the applied load during crack extension, assuming a flat crack growth resistance curve.

To determine the fracture toughness of the spray-formed deposits of $MoSi_2$ and $MoSi_2$/Ta, test samples were machined with the chevron notch oriented in two different directions. The first orientation aligned the v-notch in the spray direction whereas the second orientation aligned the v-notch parallel to the substrate, Figure 2. Both chevron notch orientations measured the fracture toughness/crack propagation through the thickness of the spray deposit but along different crack path directions.

Fracture toughness measurements were done on as-deposited material and after the deposits were hot isostatically pressed (HIP) at 1200 °C/206 MPa for 1 hour. The spray deposits were HIP'd at this condition in order to diffusion bond the individual splat layers which make up the bulk of the sprayed forms. A comparison of fracture toughness between the as-deposited material and after hot isostatic pressing was done to evaluate the influence of the as-sprayed microstructure on fracture toughness. HIP'ing conditions for this investigation were based on a diffusion couple study between $MoSi_2$ and Ta which identified a temperature at which a minimal reaction layer of $(Mo,Ta)_5Si_3$ formed between $MoSi_2$ and Ta [9].

Chevron 4-point bend samples were subsequently tested on an Instron using a constant crosshead speed of 0.050 mm/min during loading. Load-displacement data was taken using an X-Y strip chart recorder from which the maximum loads (P_{max}) were determined graphically.

3.0 Results and Discussion

3.1 Microstructure

The microstructure of the spray-formed deposits consisted of a layered assembly of impacting splats which were approximately 3 to 4 micrometers thick. These individual splats make up the bulk of the deposit and create a very convoluted array of layers with varying orientations. This array of splat layers can be compared to a brickwall structure which consists of many intricate interlocking splats and partially melted particles. The complex 3D brickwall structure associated with the as-sprayed $MoSi_2$ and the $MoSi_2$-20 w/o Ta are given in Figures 3 and 4. The presence of the well defined splat layers in these figures is evidence of a lack of remelting of the just-solidified splat surfaces by subsequent impacting particles.

A TEM image of the as-sprayed $MoSi_2$ deposit shows the fine equiaxed grains (0.2 to 3 micrometers) which results from the rapid solidification that occurs after impacting and spreading of the individual particles, Figure 5. Since the average thicknesses of the splat layers are approximately 3 micrometers, a number of grains can exist through the thickness of an individual splat. This is demonstrated in a cross-sectional TEM image of the spray deposit, Figure 6. Grain sizes of this order have been shown to increase the fracture toughness by minimizing dislocation pile-up stresses in each grain [13].

The tantalum phase distribution within the $MoSi_2$/Ta sprayed-forms is seen as a uniform distribution of discontinuous tantalum lamelli with a small percentage of unmelted tantalum powder particles, Figure 4. The volume fraction of the tantalum phase in the $MoSi_2$/Ta deposits corresponds to approximately 10 $\pm$ 2.3 v/o for the 10 w/o tantalum loaded deposit and 20 $\pm$ 1.8 v/o for the 20 w/o tantalum loaded deposit. These volume fractions were determined using a Tracor Northern 5500 Image Analysis Program (Vista) at ten different locations within the spray deposits. Volume fractions of tantalum in the spray deposits were believed to be higher than expected due to segregation of $MoSi_2$ and Ta feedstock powders during powder injection into the plasma jet.

3.2 Fracture Toughness

The resulting array of individual splats and splat boundaries which make up the spray-formed deposits, along with the discontinuous tantalum additions, have resulted in a significant increase in fracture toughness for both the $MoSi_2$ and the $MoSi_2/Ta$ deposits. Results from the chevron notch 4-point bend tests in both orientations ie., the sprayed direction and perpendicular to the sprayed direction, have shown increases in fracture toughness from (4.50 ± 0.173 MPa $m^{1/2}$) for as-sprayed $MoSi_2$ to (9.97 ± 0.351 MPa $m^{1/2}$) for the $MoSi_2$ with the 20 w/o loading of tantalum, Figure 7. This increase in fracture toughness was observed in both the as-sprayed condition and after hot isostatic pressing at 1200 °C/206 MPa for 1 hour. In addition, fracture toughness results for the as-sprayed $MoSi_2$ were comparable to that which has been reported for conventional hot pressed $MoSi_2$ [14].

Figures 8 and 9 show cracks radiating from the corners of hardness indents in $MoSi_2$ and the $MoSi_2$-20 w/o Ta spray deposits. The crack/microstructure interactions that contributed to the observed increases in fracture toughness are evident in these figures. Crack deflection, microcracking, crack blunting, and crack bridging all occur as a result of the layered microstructure in the spray deposits and the ductile tantalum additions. Anisotropic crack behavior is also shown to exist within the spray-formed deposits [15]. Cracks that propagated in the spray direction followed a more tortuous path due to crack deflections that occurred along individual splat interfaces. Cracks that propagated along the plane of the splats, however, caused separation of individual splat boundaries and splat surfaces. After Hip'ing the spray deposits, a more isotropic crack behavior resulted due to the bonding that occurred between individual splats. Chevron notched 4-point bend tests showed a decrease in fracture toughness of $MoSi_2$ after Hip'ing when compared to the fracture toughness results in the as-sprayed condition (4.5 MPa $m^{1/2}$ to 3.8 MPa $m^{1/2}$), Figure 7.

3.3 Fracture Analysis

The fracture surfaces that were created during the chevron notch 4-point bend tests were used to characterize the fracture modes of the $MoSi_2$ and $MoSi_2$/Ta deposits in both the as-sprayed condition and after hot isostatic pressing. One fracture feature that was characteristic of both the as-sprayed $MoSi_2$ and the as-sprayed $MoSi_2$/Ta composites was the interlaminar fracture that occurred along individual splat boundaries and splat surfaces. In Figure 10, the fracture surface of as-sprayed $MoSi_2$ clearly shows the interlaminar separation that has occurred along individual splat boundaries. Although this type of fracture seems to dominate the fracture surface of the $MoSi_2$, both transgranular cleavage and intergranular fracture are also present within the individual $MoSi_2$ splat layers. These fracture characteristics appear to correspond to the microstructural features within each individual splat layer.

Both these fracture modes are characteristically low-energy mechanisms which can operate simultaneously when the resolved stresses for grain-boundary separation and transgranular cleavage are approximately equal. After hot isostatically pressing of $MoSi_2$, the well defined splat interfaces in the as-deposited condition have been reduced due to the diffusion bonding that occurred between adjacent splat layers, Figure 11.

In analyzing the fracture surface of the $MoSi_2$/Ta deposits, the characteristic appearance of the discontinuous tantalum splat layers showed regions of plastic flow and necking which appeared as ductile tear ridges perpendicular to the surface of the individual splats, Figure 12. The presence of these ductile tear ridges have been defined by a mechanism of local fracture that occurs at a discontinuity in crack advancement between two different fracture modes [16]. For the two-phase system of $MoSi_2$ and tantalum, differences in mechanical properties will result in this discontinuity in fracture modes resulting in a difference in crack advancement through the $MoSi_2$ matrix.

After the $MoSi_2$/Ta deposits were HIP'd at 1200 °C/206 MPa for 1 hour, diffusion bonding between individual splats resulted in a reduction of interlaminar fracture along the splat boundaries and splat surfaces, Figure 13. This feature was consistent with the fracture surface that was produced after hot isostatic pressing the as-deposited $MoSi_2$. An intermediate reaction layer between $MoSi_2$

and tantalum splats was found after hot isostatic pressing. This reaction layer is believe to be $(Mo,Ta)_5Si_3$ which forms around 1100 °C [17]. Along this layer, there was evidence of good bonding between the tantalum and $MoSi_2$ layers, although some delamination resulted in this region, Figure 13.

Conclusion

In this investigation, low pressure plasma spraying was employed as a method for fabricating both monolithic and ductile reinforced composites of $MoSi_2$. When combining the intricate network and complex layering of the spray-formed deposits with the high strain to failure of the discontinuous ductile reinforcement, substantial increases in fracture toughness where achieved for the ductile reinforced $MoSi_2$ composite. Fracture toughness results from this study were comparable to that which has been reported for conventional hot pressed $MoSi_2$. In addition to the fracture toughness benefits that resulted from this study, a marked anistropy in fracture toughness was observed as a result of the presence of splat boundaries.

10. T.T. Shih, *American Society for Testing of Materials, Engineering Fracture Mechanics*. 14(4) (1981) 821.

11. D. Munz, R.T. Bubsey, and J.L. Shannon, *J. Am. Cerm. Soc.* 63(5-6) (1980) 300.

12. D. Munz, J.L. Shannon, and R.T. Bubsey, *Inter. Journal of Fracture*. 16(4) (1980) 300.

13. I. Baker, and P.R. Munroe, *J. of Metals*. 40(2) (1988) 28.

14. D. H. Carter, M.S. Thesis, Massachuscetts Institute of Technology, (1988).

15. R.G. Castro, R.W. Smith, A.D. Rollett and P.W. Stanek, *Scripta Metal.*, in press.

16. J.A. Fellows, *Fractography and Atlas of Fractographs*, American Society for Metals, 8th Edition, Vol. 9, Metals Park, OH, (1974) 251.

17. E. Fitzer and F. K. Schmidt, *High Temperature and Pressures*. 3 (1971) 445.

10. T.T. Shih, *American Society for Testing of Materials, Engineering Fracture Mechanics*. 14(4) (1981) 821.

11. D. Munz, R.T. Bubsey, and J.L. Shannon, *J. Am. Cerm. Soc.* 63(5-6) (1980) 300.

12. D. Munz, J.L. Shannon, and R.T. Bubsey, *Inter. Journal of Fracture*. 16(4) (1980) 300.

13. I. Baker, and P.R. Munroe, *J. of Metals*. 40(2) (1988) 28.

14. D. H. Carter, M.S. Thesis, Massachuscetts Institute of Technology, (1988).

15. R.G. Castro, R.W. Smith, A.D. Rollett and P.W. Stanek, *Scripta Metal.*, in press.

16. J.A. Fellows, *Fractography and Atlas of Fractographs*, American Society for Metals, 8th Edition, Vol. 9, Metals Park, OH, (1974) 251.

17. E. Fitzer and F. K. Schmidt, *High Temperature and Pressures*. 3 (1971) 445.

Table 1.

Optimized plasma spray parameters for producing spray-form deposits of $MoSi_2$ and $MoSi_2$-Ta composites.

Plasma Torch (Plasmadyne)	SG-100
Current (Amps)	950
Voltage (Volts)	50
Arc Gas Flow Rate - Argon (SLPM)	50
Secondary Gas Flow Rate - Helium (SLPM)	40
Powder Gas Flow Rate - Argon (SLPM)	10
Gas Injector	Forward
Powder Feed Rate (lbs/hr)	1.5
Spray Distance (cm)	16
Substrate Traverse Rate (mm/sec)	20
Atmosphere (MPa)	.39
Average Torch Efficiency (%)	52
Average Net Plasma Energy (kw)	25

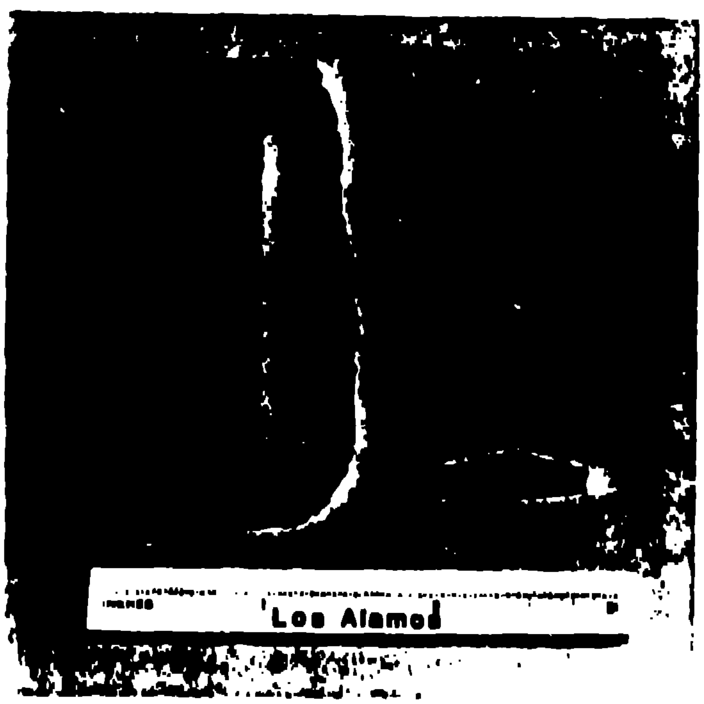

Figure 1. Representative spray deposit produced by the low pressure plasma spray process.

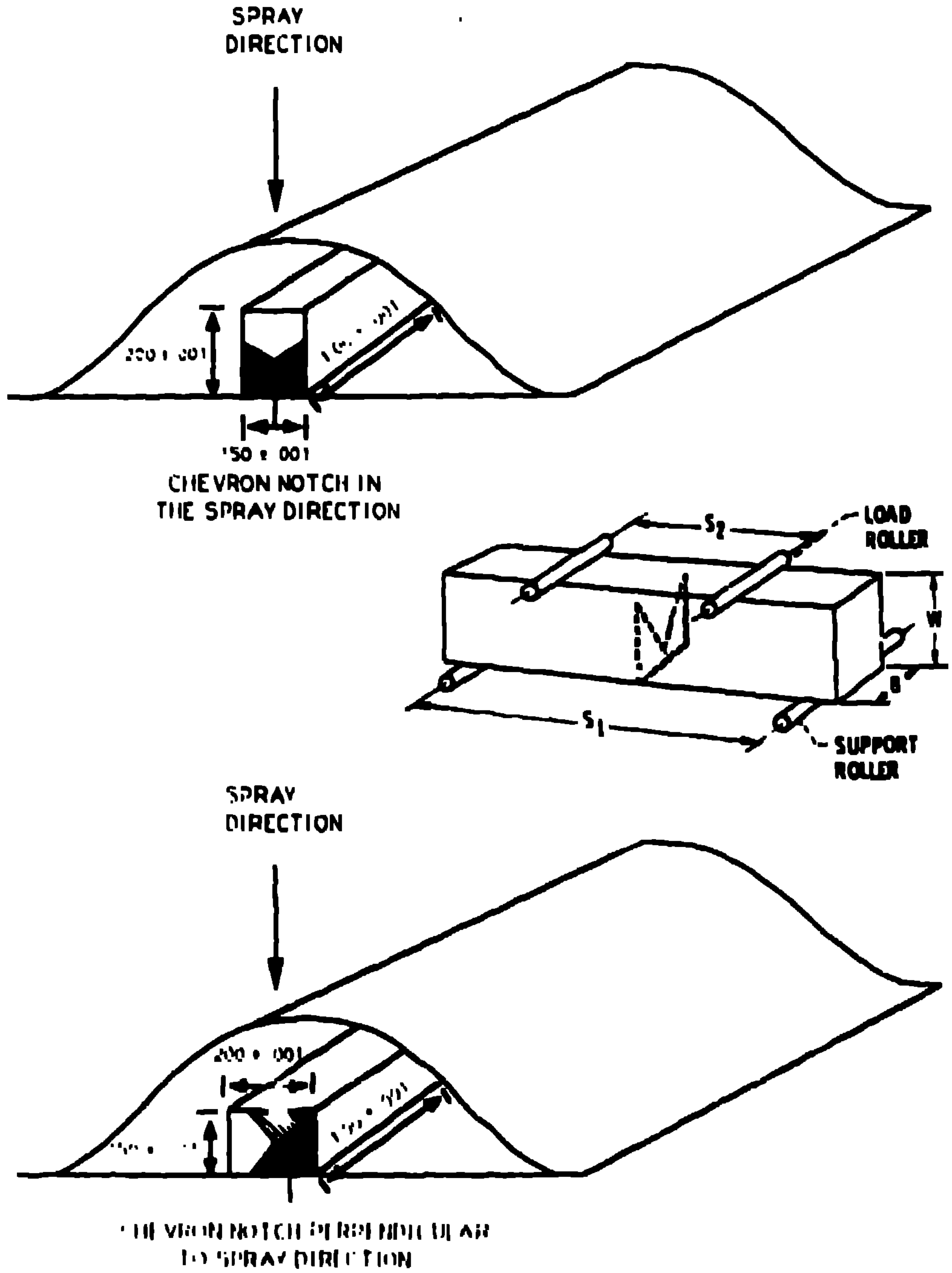

Figure 2. Chevron V-notch test orientation in the spray-formed deposits.

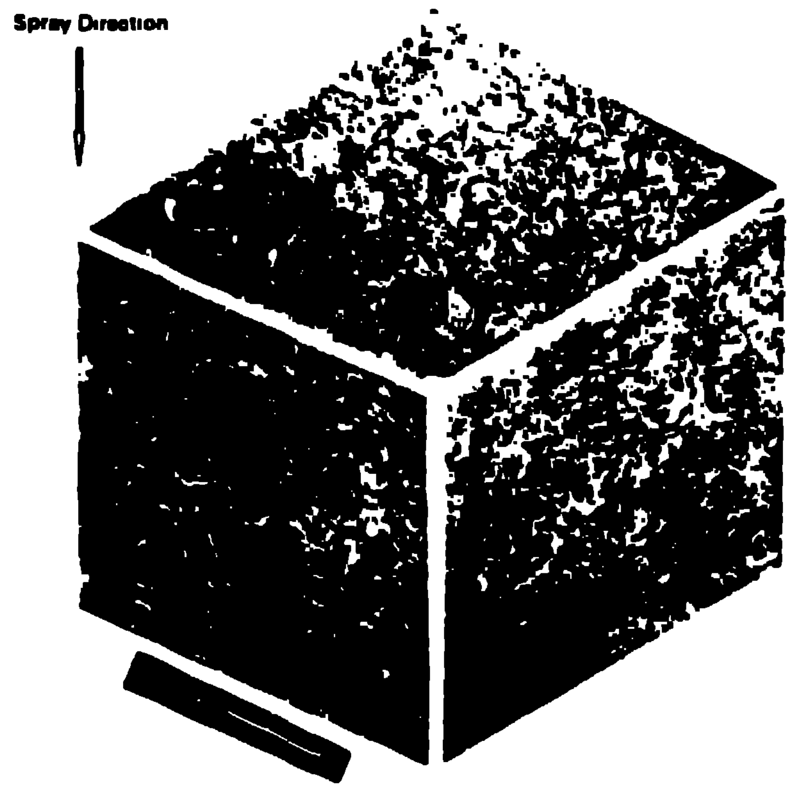

Figure 3. 3-D image of as-sprayed MoSi showing assembly of impacting splats of MoSi (gray phase) and Mo-rich regions (light phase) which makeup the bulk of the deposit.

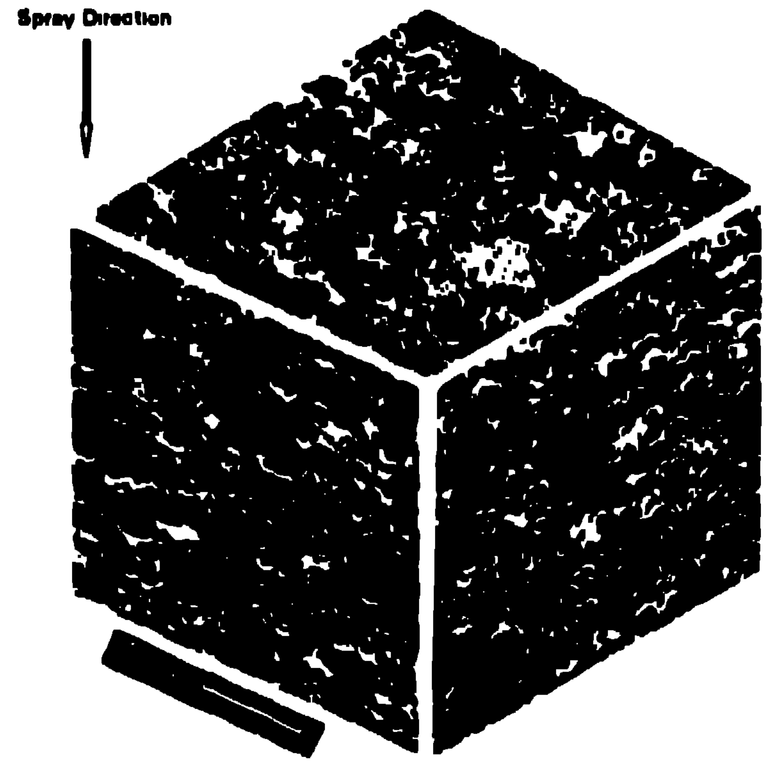

Figure 4. 3-D image of MoSi -20 w/o Ta showing individual splats of MoSi (gray phase) and tantalum (white phase) which make up the bulk of the deposit.

Figure 5. TEM bright field image showing fine equiaxed grains (0.5 to 3 micrometers) in the MoSi deposit.

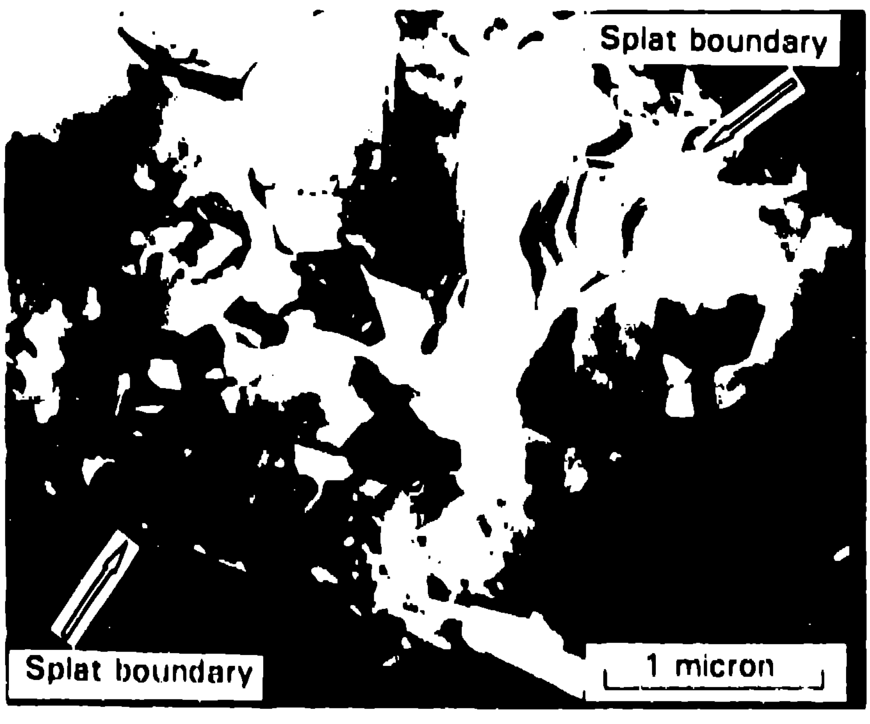

Figure 6. TEM cross section of an individual splat layer showing a range of grain sizes (0.2 to 2 micrometers) through the thickness of a MoSi splat.

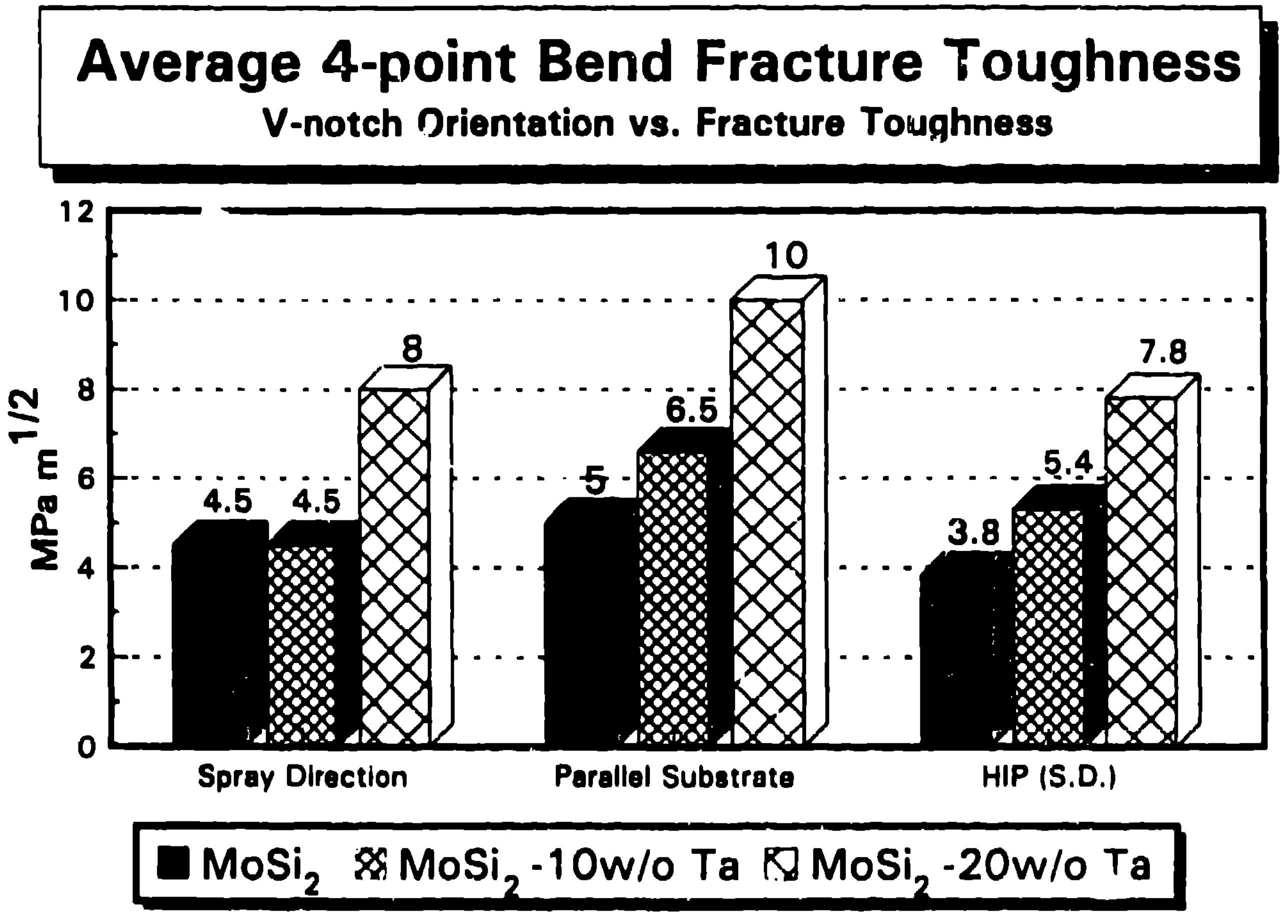

Figure 7. Results of chevron 4 point bend test before and after hot isostatic pressing at 1200 °C/206 MPa for 1 hour.

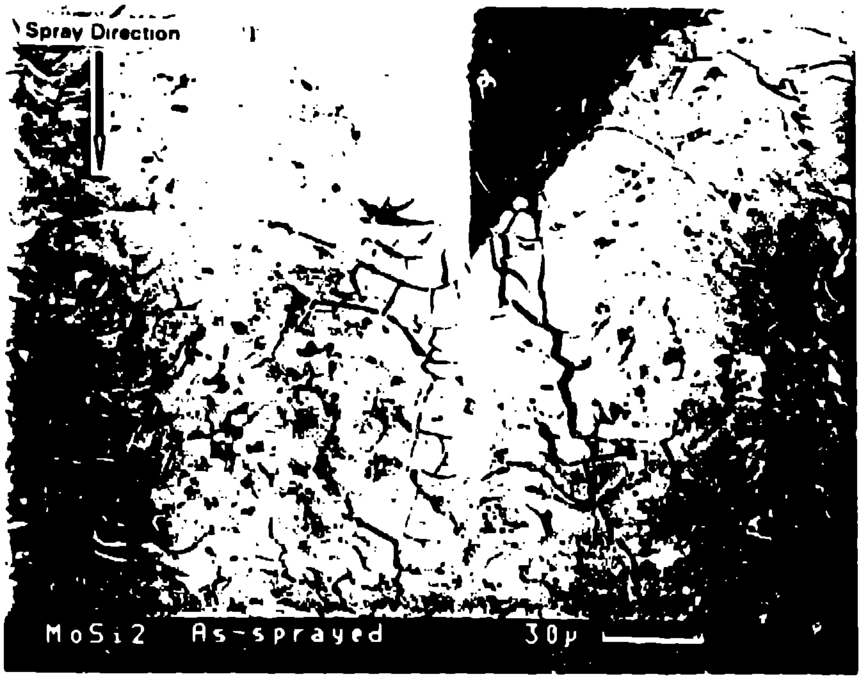

Figure 8. Microhardness indent into $MoSi_2$ illustrating the crack/microstructure interactions which result in microcracking, crack deflection and crack blunting.

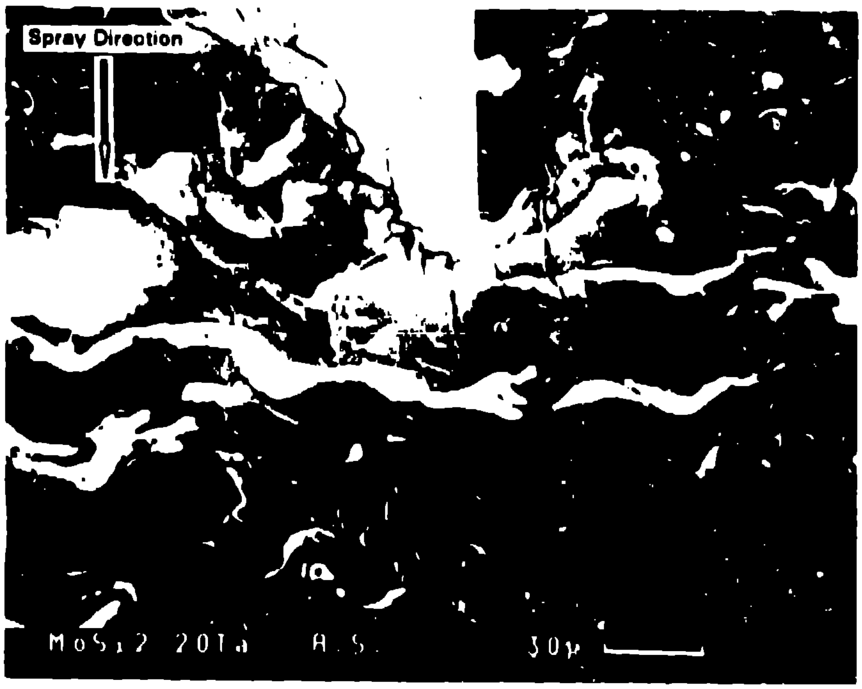

Figure 9. Microhardness indent into $MoSi_2$ 20 w/o Ta illustrating the crack/tantalum interactions which result in crack blunting, crack bridging and crack deflection.

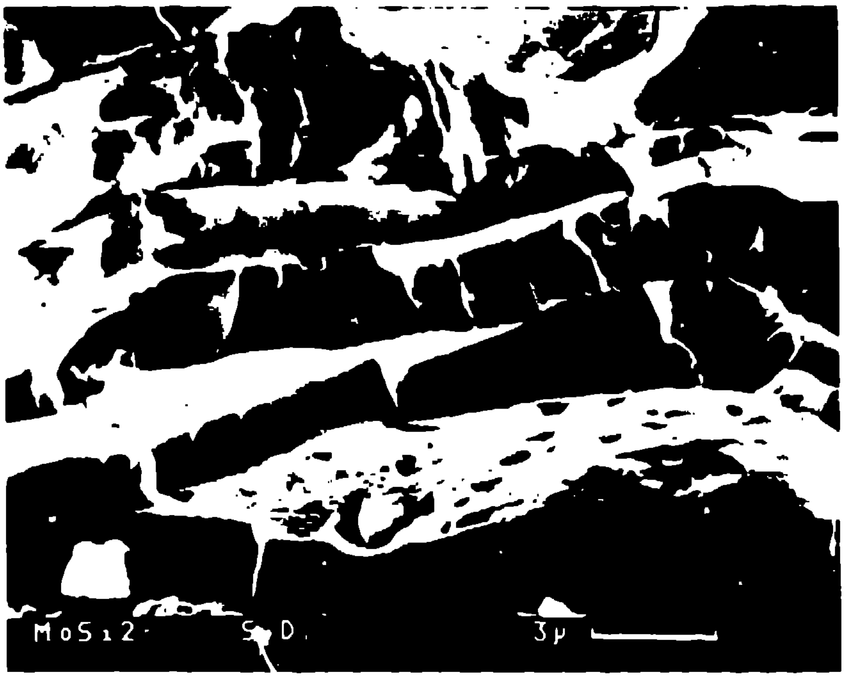

Figure 10. Interlaminar fracture along individual splat boundaries and splat surfaces in as-sprayed $MoSi_2$.

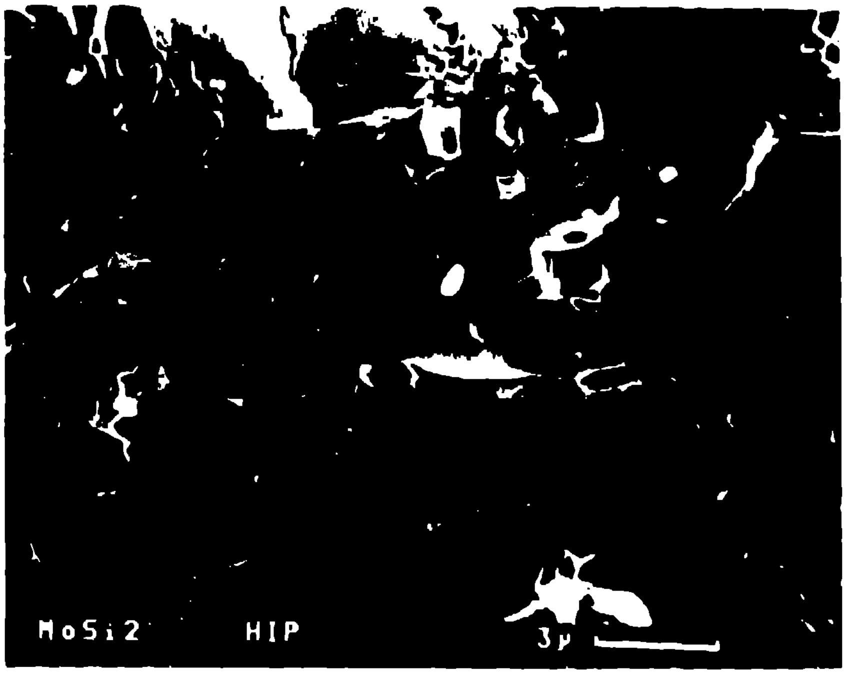

Figure 11. Reduction of interlaminar fracture in as sprayed $MoSi_2$ after HIP'ing at 1200 °C/206 MPa for 1 hour.

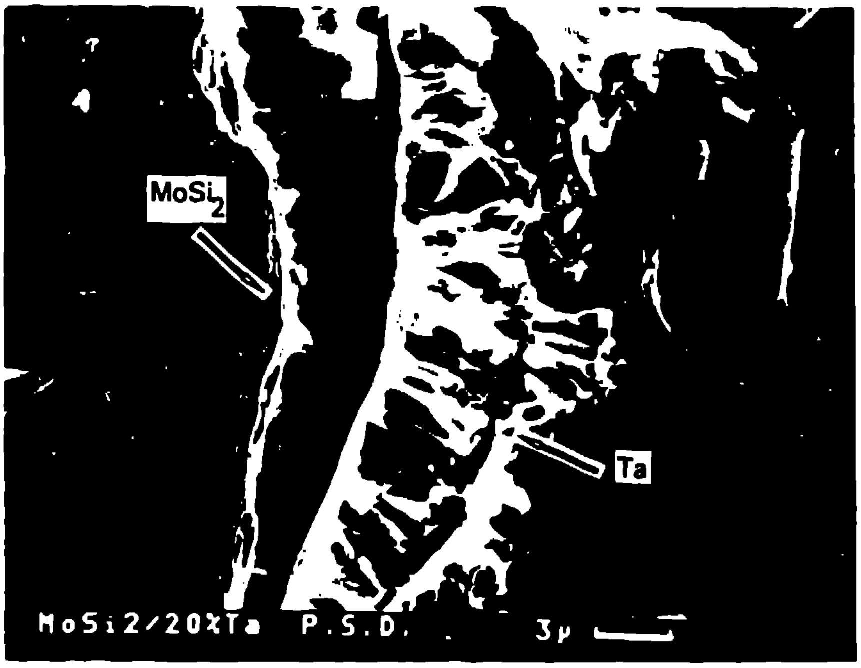

Figure 12. Fracture surface of as-sprayed $MoSi_2$-20 w/o Ta showing difference in the fracture modes of $MoSi_2$ and Ta.

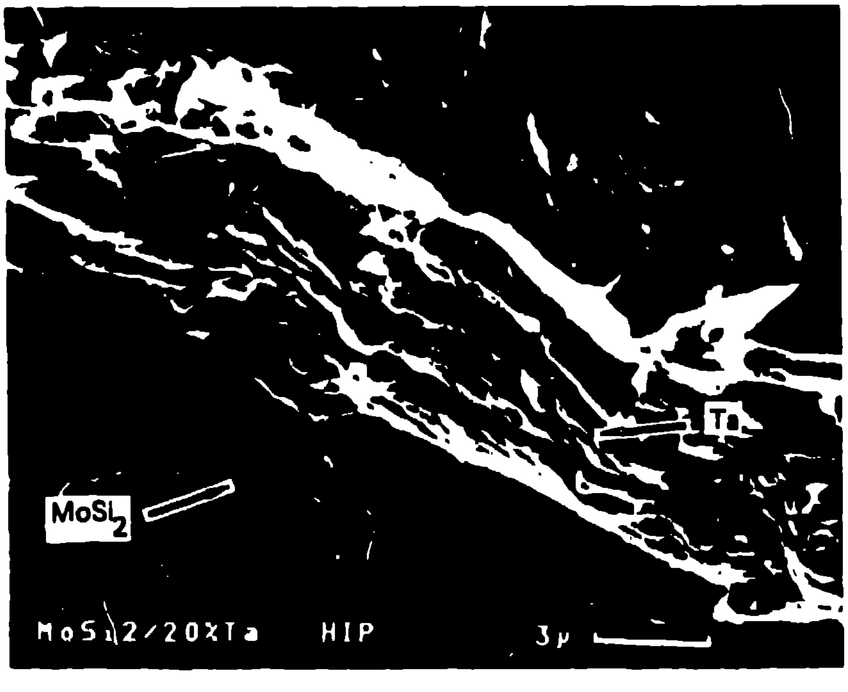

Figure 13. Fracture surface of $MoSi_2$-20 w/o Ta showing diffusion bonding between the $MoSi_2$ and Ta splat layers after HIP'ing at 1200 °C 206 MPa for 1 hour.